Ab Initio Molecular Dynamics Simulation of Liquid CdTe and GaAs: Semiconducting versus Metallic Behavior

Vitaliy V. Godlevsky, Jeffrey J. Derby, and James R. Chelikowsky
Department of Chemical Engineering and Materials Science, Minnesota Supercomputer Institute, University of Minnesota, , Minneapolis, Minnesota 55455
(Received 13 May 1998)

All semiconductors of group IV, such as silicon, and III-V materials, such as gallium arsenide, assume metallic behavior when melted. This is in contrast to some II-VI semiconductors such as CdTe which retain their semiconducting behavior in both the liquid and the solid state. In order to understand this difference, we have performed *ab initio* molecular dynamics simulations of liquid GaAs and CdTe. Using the Kubo-Greenwood formalism, we predict the conductivity of both liquids and confirm the differences observed experimentally. We relate the conductivity differences between II-VI and III-V semiconductors to strong structural differences occurring within the melt. [S0031-9007(98)07783-7]

PACS numbers: 72.80.Ph, 31.15.Ar, 71.15.Pd

First-principles studies of liquid semiconductors have received considerable attention within the past decade. Numerous *ab initio* molecular dynamics simulations of IV (Si and Ge [1–3]) and III-V (GaAs, [4], GaSb [5]) liquid semiconductors have been performed. However, II-VI semiconductors have not attracted such attention. To our knowledge, there have been no first-principles simulations performed for liquid II-VI semiconductors. This is unfortunate, as experiments suggest that II-VI materials exhibit properties which are fundamentally different from IV and III-V semiconductors in the liquid phase. From experiment, [6], CdTe remains a semiconductor in the melt as the electrical conductivity grows with increasing temperature.

An empirical rule [7] suggests that a molten semiconductor retains its semiconductor properties despite the destruction of long range order only if the short range order of the crystalline phase is preserved. Indeed, the entropy change for the solid $\rightarrow$ liquid phase transformation in CdTe is small compared to III-V semiconductors [8]. This entropy difference implies that the structural changes occurring when CdTe melts are smaller than for III-V systems. Neutron scattering experiments reinforce this picture [9]. These measurements have been interpreted to indicate that liquid CdTe (*l*-CdTe) preserves its crystalline local environment with a coordination number of $\sim$4. This is in contrast to the more close-packed structures of liquid IV and III-V semiconductors. Coordination numbers in these liquids change from 4 in the crystalline phase to $\sim$6 in the liquid phase. The degree of dissociation is another difference, in *l*-CdTe it is noticeably lesser than in liquid III-V compounds [10]. In *l*-CdTe there are fewer "wrong bonds," i.e., bonds between like-atoms. The large degree of dissociation in liquid III-V semiconductors can be thought of as increasing the random mixing of different type atoms.

Here we compare structural and electronic properties of *l*-CdTe with *l*-GaAs, a typical representative of III-V semiconductors. In our simulations, we model the liquid ensemble with a 64-atom supercell geometry. The supercell corresponds to a cubic zinc-blende structure with a doubled lattice constant. During simulations, the sizes of the supercells were constrained to experimental densities of the melt, i.e., we fixed our supercell size to be 25.28 Å and 20.86 Å for *l*-CdTe and *l*-GaAs, respectively [4,9].

To prepare the liquid ensemble, we first melt the semiconductor by pumping energy into the system via Langevin dynamics [11–13]. The time steps used in integrating equations of motion were 200 a.u. and 300 a.u. (1 a.u. = 2.4×10^{-17} s) for GaAs and CdTe systems, respectively. The interatomic forces are computed quantum mechanically from *ab initio* pseudopotentials with a plane wave basis set [12]. We used a Troullier-Martins [14] pseudopotential with Ceperly-Alder correlation [15]. The Cd 4*d* electrons are treated as core electrons using a partial core correction [16]. We used an energy cutoff of 12 Ry for CdTe plane wave basis. For GaAs we use 10 Ry for the cutoff energy. The Brillouin zone was sampled at the Γ point to determine the charge density.

Initially our liquid ensemble consists of a random arrangement of atoms within the supercell. We thermalized the initial configuration at a temperature of 6000 K. This "hot" temperature regime eliminates any "memory" effect from the initial state. After a time for the average diffusion path of the atoms to be comparable with the conventional lattice constant (1.7 ps and 2 ps for GaAs and CdTe, respectively), we cool the system to the final equilibrium temperature. The cooling process was done over a 2 ps interval. The final temperatures, 1550 K for GaAs and 1370 for CdTe, were fixed to be just above the melting points. When the desired temperatures were obtained we turned off the Langevin dynamics and we decoupled our system from the hypothetical heat bath. To construct a representative ensemble, we ran simulations for 3 ps for each system following Newtonian dynamics.

From the atomic coordinates of the liquid ensemble, we calculated the total and partial radial distribution functions by averaging over the simulation time. From the partial

radial distribution functions via a Fourier transformation, we obtained the partial structure factors. The total structure factor is a linear combination of the partial structure factors normalized by the neutron scattering lengths [4]. We can compare the calculated structure factor with neutron scattering experiments. We assume the experimental scattering length ratios: $\alpha_{\mathrm{Ga}}/\alpha_{\mathrm{As}} = 7.2/6.7$ for GaAs, and $\alpha_{\mathrm{Cd}}/\alpha_{\mathrm{Te}} = 5.8/7.5$ for CdTe in making these comparisons [17].

In Fig. 1, we show the experimental and theoretical structure factors for *l*-GaAs and *l*-CdTe, as well as the total radial distribution functions. We compare our structure factor for *l*-CdTe with experimental data [9] and the theoretical result obtained by molecular dynamics simulations based on a Stillinger–Weber-type classical potential [18]. For *l*-CdTe, there is a left shoulder on the first peak at ~ 2 Å^{-1} in all three curves. For the first peak and the shoulder, our *ab initio* simulations agree better with experiment than do the classical simulations [18]. For the second peak, the agreement with the experiment is quite good for both theoretical simulations. The total radial distribution for *l*-CdTe has a more pronounced first and second shell structure in contrast to the distribution function for *l*-GaAs. We attribute this difference to a more random structure of the melt in GaAs.

From the total and partial radial distribution functions, we can estimate coordination numbers as $C_{\alpha\beta} = \int_0^{R_{\min}} 4\pi r^2 g_{\alpha\beta}(r)\, dr$, where $R_{\min}$ is the first minimum coordinate in the total radial distribution function $g(r)$. For the $R_{\min}$ we take 3.5 Å and 3.3 Å for the CdTe and GaAs systems, respectively. The total coordination number for *l*-CdTe is 4.4. In contrast to *l*-CdTe, *l*-GaAs assumes a close-packed structure with a coordination number of 6.4. To estimate compositional defects, we introduce a compositional disorder number (CDN) defined as $(C_{\mathrm{anion-anion}} + C_{\mathrm{cation-cation}})/2C_{\mathrm{anion-cation}}$. The compositional disorder number can also be thought of as an order parameter. For example, for zinc-blende structure, CDN is 0 while, for a perfect random mix, CDN is 1. In *l*-CdTe, there are fewer wrong bond defects than in *l*-GaAs. CDN = 0.4 for *l*-CdTe as opposed to more disordered, or randomly mixed, *l*-GaAs with CDN = 0.8. In the total angular distribution for *l*-GaAs (Fig. 2), there are two major peaks comparable in the amplitude. One peak ($\sim 60°$) corresponds to close-packing structure, while the other peak ($\sim 100°$) relates to tetrahedral environment. In *l*-CdTe the tetrahedral peak dominates. The tetrahedral coordination and a low composition disorder number indicate that CdTe retains its short range order upon melting. This agrees with the small entropy change measured in the solid-liquid transition [8].

During the simulations, we were able to observe that atoms of Te form branched chains. Experiment and theoretical simulations, [20,21] suggest that, in pure liquid Te, atoms of Te form twofold coordinated helicon chains. It is interesting that this ability to form chains is preserved in *l*-CdTe. In Fig. 3, we illustrate the structure of Te clusters in a typical *l*-CdTe atomic configuration. Two atoms are considered to form a bond if the distance between them is less than the first minimum in the total

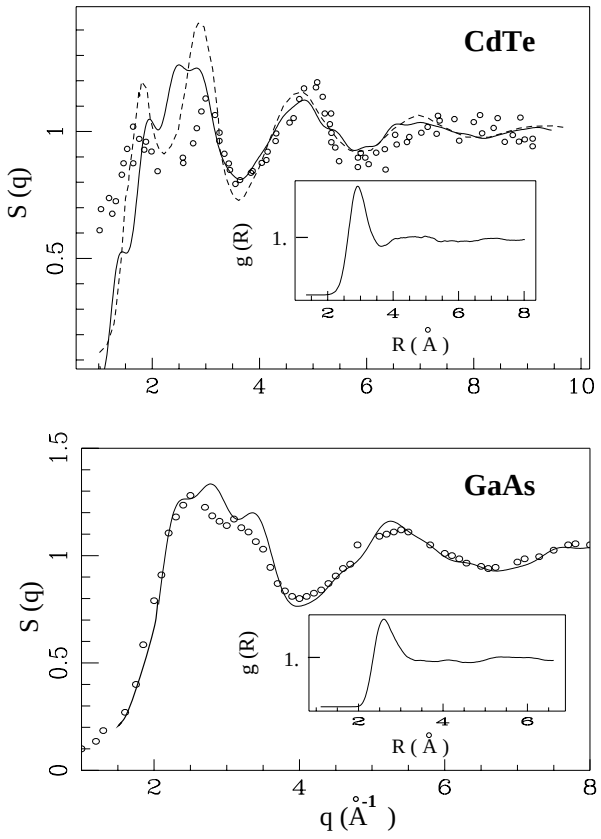

FIG. 1. Structure factor functions, $S(q)$, and total radial distributions, $g(R)$, for *l*-CdTe and *l*-GaAs: theory (solid lines) compared to experiment [9,19] (circles). For *l*-CdTe the dashed line presents the result obtained with Stillinger-Weber potential simulations [18].

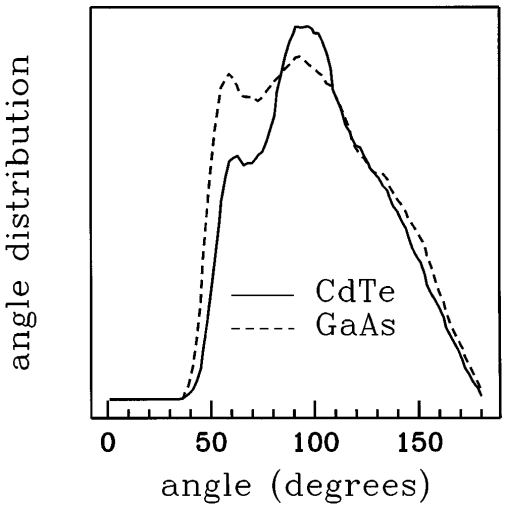

FIG. 2. Total angular distributions for *l*-Cdte and *l*-GaAs.

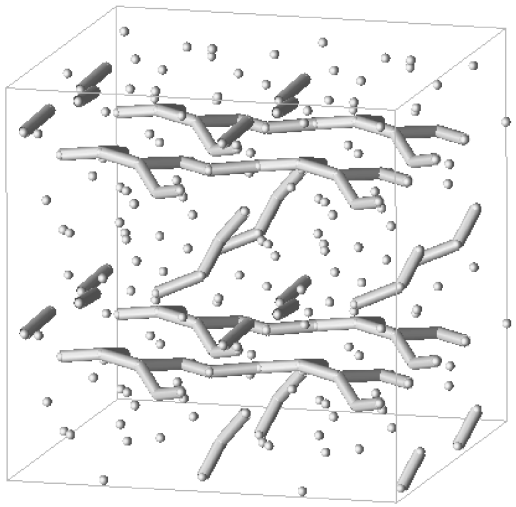

FIG. 3. Atoms of Te form branched chains in *l*-CdTe (only Te atoms and bonds between them are presented). The shown geometry corresponds to the $2 \times 2 \times 2$ supercell configuration.

radial distribution function, $R_{\min}$. These compositional defects, bonds between Te atoms, contain only 45% of all Te atoms. The rest of the Te atoms are not bonded with each other. Cd clusters are more complex. There are triplets, more complex rings, and even tetrahedrons of Cd atoms in the liquid.

In the bond angular distribution of Te clusters, there are two well-distinguished peaks (see Fig. 4). One peak corresponds to the "open" angle in the helicon chains, at approximately 160°. The other peak, located at ~100°, corresponds to the chain branching. In the bond angular distribution of the more complex Cd clusters, a tetrahedral angle at ~100° prevails.

Once the eigenfunctions are obtained from the Kohn-Sham equation, we can calculate the optical conductivity. According to the Kubo-Greenwood expression [22], the real part of the conductivity can be expressed as

$$\sigma_r(\omega) = \frac{2\pi e^2}{3m^2\omega\Omega} \sum_{n,m} \sum_{\alpha=x,y,z} |\langle\psi_m|p_\alpha|\psi_n\rangle|^2 \times \delta(E_n - E_m - \hbar\omega), \quad (1)$$

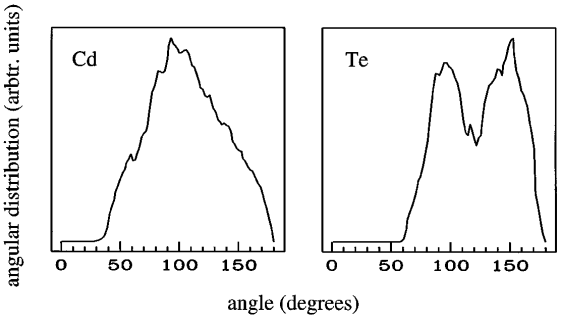

FIG. 4. Partial angular distributions for bonds in Te and Cd clusters.

where E_i and ψ_i are eigenvalues and eigenfunctions, and Ω is the volume of the supercell. Dipole transition elements, $\langle\psi_m|p_\alpha|\psi_n\rangle$, were sampled by the Γ point of the Brillouin zone. The lowest 300 eigenstates are included in the summation.

In Fig. 5, we display the real part of optical conductivity calculated for *l*-CdTe and *l*-GaAs. Each curve is the result of the conductivity averaged over configurations chosen at random from the representative ensemble. Typically, only 5–10 configurations are required to obtain a converged conductivity. The calculated conductivity is smoothed by convoluting it with a 0.3 eV Gaussian (full width half maximum). The dc conductivity value (at $\omega = 0$) is linearly extrapolated from $\omega \to 0$. For *l*-GaAs, the dc conductivity is 8600 $\Omega^{-1}\,\mathrm{cm}^{-1}$, compared with the experimental value, 7900 $\Omega^{-1}\,\mathrm{cm}^{-1}$ [6]. For *l*-CdTe, the dc conductivity is 100 $\Omega^{-1}\,\mathrm{cm}^{-1}$. This value overestimates the conductivity when compared to the experimental value of 40 $\Omega^{-1}\,\mathrm{cm}^{-1}$ [6]. Nonetheless, the static conductivity of *l*-GaAs is almost 2 orders of magnitude larger than that of *l*-CdTe.

The behavior of conductivities of *l*-CdTe and *l*-GaAs is quite different as ω approaches 0. While *l*-GaAs has Drude-like conductivity [$\sigma(\omega) \sim \sigma_0/(1 + \omega^2\tau^2)$] which is common for metals, *l*-CdTe conductivity has a semiconductor character. After peaking at 4 eV, the conductivity for *l*-CdTe decreases as the frequency decreases. This behavior indicates that there is a finite band gap in the density of states for *l*-CdTe.

We do not expect perfect agreement with the experimental data. For example, our calculated optical conductivity does not include scattering by phonons or impurities. Another approximation is our use of the Kohn-Sham eigenvalues to estimate the excitation spectrum. We expect that the "band gap" problem will affect

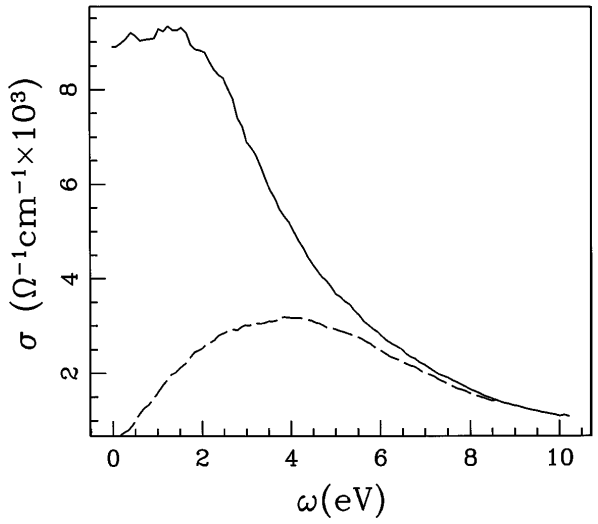

FIG. 5. Optical conductivity in *l*-GaAs (solid line) and *l*-CdTe (dashed line).

optical properties for small ω. With the pseudopotentials we use, local density approximation underestimates the band gap for CdTe more than for GaAs. This can partially account for the larger error in the dc conductivity of *l*-CdTe. On the other hand, the accuracy of the experimental data for the dc conductivity is also problematic. Values for *l*-CdTe vary by a factor of 2 in the literature [6,23,24].

From the real part of the conductivity, using the Kramers-Kronig relations, we can obtain the imaginary part of the conductivity. Dielectric constant can be obtained from the electrical conductivity:

$$\epsilon(\omega) = 1 + \frac{4\pi i}{\omega}\,\sigma(\omega)\,. \qquad (2)$$

We can calculate optical properties such as reflectivity and the attenuation coefficient. There are no extensive measurements of the reflectivity of *l*-CdTe. However, using an Ar^+ laser ($\lambda = 488$ nm) to measure the reflectivity in laser induced melted CdTe, Golovan *et al.* [25] have observed the reflectivity to increase by 30% upon melting of CdTe. If the experimental reflectivity of crystalline CdTe is increased by 30%, the reflectivity of the liquid is 0.35. This value is in excellent agreement with our calculated reflectivity for *l*-CdTe, the value of which is also 0.35. This increase in reflectivity for CdTe is substantially less than the change observed for III-V and IV semiconductors, and is consistent with the less metallic behavior of the CdTe melt. From our calculations, the normal incident reflectivity of *l*-GaAs exceeds the reflectivity of *l*-CdTe by almost a factor of 2 for photon energies less than 5 eV.

In conclusion, we believe that differences in the conductivity and optical properties of *l*-CdTe and III-V (or IV) liquid semiconductors can be assigned to differences in bond ionicity and the corresponding structural differences. In IV or III-V semiconductors, with higher temperatures, entropy favors a disordered and close-packed structure (entropy is larger for such configurations). Consequently, a transition occurs from a fourfold structure to a more randomly mixed and a denser sixfold coordinated structure. In *l*-CdTe, the higher ionicity of anion-cation bonds does not favor proximity of like atoms. This restricts the miscibility of different types of atoms and causes long range correlation in partial radial distributions for like atoms. The higher ionicity of Cd-Te bonds limits the delocalization of electrons which also contributes to the semiconductor properties of *l*-CdTe. Comparison of the metallic Drude-like conductivity *l*-GaAs and the conductivity of *l*-CdTe confirms our calculated semiconductor character of *l*-CdTe. The conductivity in *l*-CdTe decreases as the frequency approaches zero. As opposed to the nearly free electron density of states in *l*-GaAs, *l*-CdTe has a finite band gap. As such, the dc conductivity for *l*-CdTe is 2 orders of magnitude less than dc conductivity of *l*-GaAs.

We would like to acknowledge the support for this work by NASA, NSF, and by the Minnesota Supercomputer Institute. Helpful discussions with S. Ögüt are acknowledged.

[1] I. Stich, R. Car, and M. Parrinello, Phys. Rev. B **44**, 4262 (1991).
[2] G. Kresse and J. Hafner, Phys. Rev. B **49**, 14 251 (1994).
[3] V. Godlevsky, J. Chelikowsky, and N. Troullier, Phys. Rev. B **52**, 13 281 (1995).
[4] Q. Zhang, G. Chiarotti, A. Selloni, R. Car, and M. Parrinello, Phys. Rev. B **42**, 5071 (1990).
[5] C. Molteni, L. Colombo, and L. Miglio, J. Phys. Condens. Matter **6**, 5255 (1994).
[6] V. Glazov, S. Chizhevskaya, and N. Glagoleva, *Liquid Semiconductors* (Plenum, New York, 1969).
[7] A. Joffe and A. Regel, *Progress in Semiconductors* (Heywood, London, 1960), Vol. 4, p. 237.
[8] B. Lichter and P. Sommelet, Trans. AIME **245**, 1021 (1969).
[9] J. Gaspard, C. Bergman, C. Bichara, R. Bellissent, P. Chieux, and J. Coffard, J. Non-Cryst. Solids **97-98**, 1283 (1987).
[10] M. Jordan, Metall. Trans. **1**, 239 (1970).
[11] R. Biswas and D. Hamann, Phys. Rev. B **34**, 895 (1986).
[12] N. Binggeli, J. L. Martins, and J. R. Chelikowsky, Phys. Rev. Lett. **68**, 2956 (1992).
[13] J. R. Chelikowsky, N. Troullier, and N. Binggeli, Phys. Rev. B **49**, 114 (1994).
[14] N. Troullier and J. L. Martins, Phys. Rev. B **43**, 1993 (1991).
[15] D. M. Ceperley and B. J. Alder, Phys. Rev. Lett. **45**, 566 (1980).
[16] S. Louie, S. Froyen, and M. L. Cohen, Phys. Rev. B **26**, 1738 (1982).
[17] J. Emsley, *The Elements* (Oxford University Press, Oxford, 1996), 3rd ed.
[18] V. Glazov and L. Pavlova, J. Cryst. Growth, **184/185**, 1253 (1998).
[19] C. Bergman, C. Bichara, P. Chieux, and J. Gaspard, J. Phys. Colloq. **C8-46**, 97 (1985).
[20] M. Yao, H. Endo, J. Non-Cryst. Solids **205-207**, 85 (1996).
[21] C. Bichara, J. Raty, J. Gaspard, J. Non-Cryst. Solids **205-207**, 361 (1996).
[22] R. Kubo, J. Phys. Soc. Jpn. **12**, 570 (1957); D. Greenwood, Proc. Phys. Soc. **71**, 585 (1958).
[23] L. Shcherbak, J. Cryst. Growth **184-185**, 1057 (1998).
[24] P. Rudolph, Prog. Cryst. Growth Charact. **29**, 275 (1994).
[25] L. Golovan, P. Kashkarov, and V. Timoshenko, J. Tech. Phys. Lett. **21**, 26 (1995).